

# Selective-Memory Meta-Learning with Environment Representations for Sound Event Localization and Detection

Jinbo Hu, *Student Member, IEEE*, Yin Cao, *Member, IEEE*, Ming Wu, *Member, IEEE*,  
Qiuqiang Kong, *Member, IEEE*, Feiran Yang, *Member, IEEE*,  
Mark D. Plumbley, *Fellow, IEEE*, Jun Yang, *Senior Member, IEEE*

**Abstract**—Environment shifts and conflicts present significant challenges for learning-based sound event localization and detection (SELD) methods. SELD systems, when trained in particular acoustic settings, often show restricted generalization capabilities for diverse acoustic environments. Furthermore, it is notably costly to obtain annotated samples for spatial sound events. Deploying a SELD system in a new environment requires extensive time for re-training and fine-tuning. To overcome these challenges, we propose environment-adaptive Meta-SELD, designed for efficient adaptation to new environments using minimal data. Our method specifically utilizes computationally synthesized spatial data and employs Model-Agnostic Meta-Learning (MAML) on a pre-trained, environment-independent model. The method then utilizes fast adaptation to unseen real-world environments using limited samples from the respective environments. Inspired by the Learning-to-Forget approach, we introduce the concept of selective memory as a strategy for resolving conflicts across environments. This approach involves selectively memorizing target-environment-relevant information and adapting to the new environments through the selective attenuation of model parameters. In addition, we introduce environment representations to characterize different acoustic settings, enhancing the adaptability of our attenuation approach to various environments. We evaluate our proposed method on the development set of the Sony-TAU Realistic Spatial Soundscapes 2023 (STARSS23) dataset and computationally synthesized scenes. Experimental results demonstrate the superior performance of the proposed method compared to conventional supervised learning methods, particularly in localization.

**Index Terms**—Sound event localization and detection, meta-learning, environment adaptation, selective memory.

## I. INTRODUCTION

Sound event localization and detection (SELD) refers to detecting categories, presence, and spatial locations of dif-

ferent sound sources. SELD was first introduced in Task 3 of the Detection and Classification of Acoustics Scenes and Events (DCASE) 2019 Challenge [1]. After three iterations of Task 3 of the DCASE Challenge [1]–[3], the types of data have transformed from computationally synthesized spatial recordings to real-scene recordings in 2022 and 2023 [4], [5]. Large-scale datasets of spatialized sound events were released for these challenges to be used for training and evaluating learning-based approaches.

### A. Learning-based SELD methods

SELD can be regarded as a multi-task learning problem. Adavanne et al. [6] proposed SELDnet for a joint task of sound event detection (SED) and regression-based direction-of-arrival (DOA) estimation. SELDnet cannot detect homogeneous overlap, which refers to overlapping sound events of the same type but from different locations. The Event-Independent Network V2 (EINV2), with a track-wise output format and permutation invariant training, was proposed to tackle the homogeneous overlap detection problem [7]–[9]. In contrast to the use of two outputs of SED and DOA in SELDnet and EINV2, the Activity-coupled Cartesian DOA (ACCCDOA) approach merges the two subtasks into a single task [10], [11], where the Cartesian DOA vectors also contain the activity information of sound events.

However, the performance of learning-based methods is usually degraded when the training set and test set are mismatched. The training set cannot cover all actual instances from different acoustic environments.

### B. Environment shifts and conflicts

The change in the data distribution between a training set and a test set is known as the domain shift problem [12], [13]. In the practical deployment of SELD systems, the differences among environments could potentially be very significant. Unseen complex acoustic environments could result in a decline in system performance, due to the distribution change in acoustic properties, such as varying degrees of echo and reverberation, diverse types of ambient noise, and directional interference. The change in the distribution of acoustic properties among environments is referred to as the environment shift. The issue is particularly salient when the system encounters acoustic properties it has not been exposed to during

Jinbo Hu, Ming Wu, and Jun Yang are with the Key Laboratory of Noise and Vibration Research, Institute of Acoustics, Chinese Academy of Sciences, Beijing 100190, China (e-mail: hujinbo@mail.ioa.ac.cn; mingwu@mail.ioa.ac.cn; jyang@mail.ioa.ac.cn). Jinbo Hu and Jun Yang are also with the University of Chinese Academy of Sciences, Beijing 100049, China. (*Corresponding author: Jun Yang*)

Yin Cao is with the Department of Intelligent Science, Xi’an Jiaotong Liverpool University, Suzhou 215123, China (e-mail: yin.k.cao@gmail.com).

Qiuqiang Kong is with the Chinese University of Hong Kong, Hong Kong, China (e-mail: qqkong@ee.cuhk.edu.hk).

Feiran Yang is with the State Key Laboratory of Acoustics, Institute of Acoustics, Chinese Academy of Sciences, Beijing 100190, China (feiran@mail.ioa.ac.cn).

Mark D. Plumbley is with the Centre for Vision, Speech and Signal Processing, University of Surrey, Guildford GU2 7XH, U.K. (e-mail: m.plumbley@surrey.ac.uk).

This work was partly supported by the National Key Research and Development Project (NO. 2022YFB2602000), Grant "XJTLU RDF-22-01-084", and Engineering and Physical Sciences Research Council (EPSRC) Grant EP/T019751/1. For the purpose of open access, the authors have applied a Creative Commons Attribution (CC BY) license to any Author Accepted Manuscript version arising.

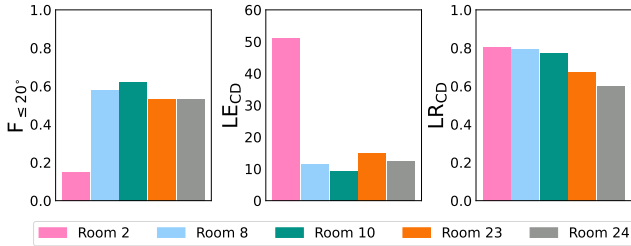


Fig. 1: Room-wise metric scores of our previous system [14] submitted to Task 3 of the DCASE 2022 Challenge on the STARSS22 validation set. The description of each metric is expounded in Section IV-B. The system obtained the second rank in the team ranking.

training. On the other hand, different acoustic environments may present conflicts. Optimal solutions for diverse acoustic environments may display considerable variation, e.g. indoor environments and outdoor environments. A single training configuration cannot encompass all types of environments.

Fig. 1 illustrates the results of our previous system [14] submitted to Task 3 of the DCASE 2022 Challenge. STARSS22 [4] is a dataset of spatial recordings of real scenes with spatiotemporal annotations of sound events. There are no duplicated recording environments between the training and test sets in STARSS22. The system was evaluated on the STARSS22 dataset and obtained second in the team ranking. However, we found unsatisfactory generalization performance for the Room 2 recordings in the *dev-test-tau* set of STARSS22 [14] compared with other rooms. Experimental results show that class-dependent localization error  $LE_{CD}$  is much higher, and location-dependent F-score  $F_{\leq 20^\circ}$  is much lower in Room 2, but class-dependent localization recall  $LR_{CD}$  is high. This suggests that our system may have weak localizing performance in Room 2 due to the environment shift or conflict.

### C. Data acquisition

One of the most effective methods for solving environment shifts and conflicts is acquiring as much data as possible [12], [13], [15]. However, manually collecting and annotating spatial sound event recordings is highly cost-intensive. For instance, the STARSS22 dataset [4] employed sophisticated setups involving a 32-channel spherical microphone array for recording, wireless microphones for manually annotating types, onset, and offset of sound events, a motion capture (mocap) system for extracting the tracked data, and a 360° camera for validating those annotations.

Another practical approach for acquiring data is computationally synthesizing spatial sound event samples. Spatial sound event recordings are simulated by convolving dry sound event samples with spatial room impulse responses (SRIRs). The multi-channel simulation (MCS) framework [16] and the impulse response simulation (IRS) framework [17] are both designed to simulate multi-channel recordings, emphasizing augmentation from original data without the reliance on external datasets. MCS and IRS involve the convolution of enhanced source signals with extracted covariance matrices

and computationally simulated SRIRs, respectively. Noteworthy among existing external datasets used for synthesizing spatial sound events include FSD50K [18], AudioSet [19], and TAU-SRIR DB [20]. FSD50K and AudioSet are large-scale sound event datasets, while TAU-SRIR DB is a real-recorded SRIR database tailored for the DCASE Challenge. Given the insufficiency of publicly accessible SELD data, particularly for specific microphone array types, e.g. the number of microphones and geometry of the microphone array, the role of the SRIR simulation technique becomes indispensable in data synthesis. Numerous RIR simulation methodologies rely on geometric approaches [21], [22], where the propagation of sound waves is modeled and manipulated in the form of a ray. These techniques simulate the reflections and reverberation of sound waves. Software packages like Pyroomacoustics [23], gpuRIR [24], and SMIR-Generator [25] are representative tools for geometric-based SRIR simulations.

### D. Meta learning

Models trained on synthetic datasets typically demonstrate a degree of generalization ability but could limit the robustness of the network on real-world data due to the environment shift [15]. One line of research is to train the model with realistic signals by transfer learning [26], pre-training a model with large-scale synthetic datasets, and then fine-tuning the model with limited real-recorded datasets [15].

In circumstances when environmental disparities occur between training sets and test sets and collected sample availability is limited, few-shot learning (FSL) [27] can offer a solution for adaptation to realistic and specific environments.

The conventional supervised learning method refers to training a model on a labeled dataset and then applying the trained model to predict unseen data. The core issue of conventional supervised learning training methodologies in the case of limited samples is that the empirical risk minimizer is unreliable [27]. Nevertheless, by incorporating prior knowledge, FSL can effectively generalize to the specific task, even with only a few samples [27]. Meta-learning, which facilitates FSL, learns a general-purpose learning algorithm that generalizes across tasks and ideally enables each new task to be learned well from the task-distribution view [28]. Meta-learning has advanced FSL significantly in computer vision [29], [30].

One of the most successful meta-learning algorithms is model-agnostic meta-learning (MAML) [31]. MAML formulates prior knowledge as commonly initialized parameters across tasks and then exploits a few samples of the target task to adapt that task quickly. Due to its model-agnostic nature, MAML is compatible with any model trained with gradient descent, making it applicable to various learning problems, including classification, regression, and reinforcement learning. In audio signal processing, the meta-learning method has recently attracted interest in solving FSL problems. Based on MAML, several audio-related researchers have investigated building systems to adapt their specific tasks rapidly with only a few corresponding samples [32]–[34]. To the best of our knowledge, the few-shot environment adaptation problems based on meta-learning have not been thoroughly studied.

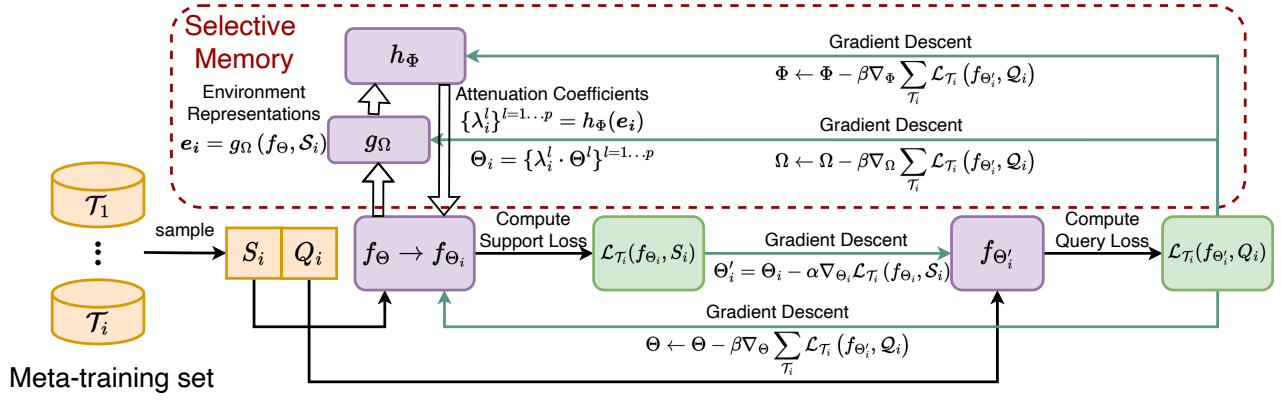


Fig. 2: A diagram of the meta-training procedure for our proposed environment-adaptive Meta-SELD. For simplicity, we only consider one gradient update for the inner loop of the training procedure.  $f_\Theta$ ,  $g_\Omega$ , and  $h_\Phi$  represent the backbone, environment extractor, and attenuation network, respectively.  $\Theta^l$ , where  $l = 1 \dots p$ , denotes the  $l$ -th layer of the total  $p$ -layer backbone  $f_\Theta$ .

MAML can be designed to employ a set of trained initial parameters and a few samples from a specific environment to cope with the environment shift problem and train multiple models for each specific environment to somewhat mitigate the environment conflict issue. However, forcibly sharing the initial parameters can still lead to some conflicts and compromises among tasks [35]. Multimodal MAML (MMAML) [36] focuses on task-dependent initial parameters and tries to learn task embeddings and transform the initial parameters with affine parameters. Compared with Multimodal MAML, Learning-to-Forget (L2F) [35] proposes layer-wise attenuation on the compromised initial parameters for each task to reduce its influence.

### E. Our contributions

In this work, we extend our previous work Meta-SELD [37] to environment-adaptive Meta-SELD, investigating an adaptation to the environment shift problem using meta-learning-based few-shot methods. Drawing inspiration from L2F [35], we propose to selectively memorize components relevant to the target environment and to learn the target environment by using environment representations. Fig. 2 presents a flow diagram of environment-adaptive Meta-SELD. In contrast to [38], which tackles unseen categories of sound events problem in SELD, our proposed Meta-SELD focuses on adaptation to unknown environments.

The method of fast adaptation to environments is mainly based on Model-Agnostic Meta-Learning (MAML) [31] and an environment-independent (EI) model. The EI model is pre-trained on a computationally synthesized dataset, encompassing a wide range of acoustic environments. We then apply MAML to the pre-trained EI model to create a meta-EI model, which enables fast adaptation to an unseen environment using a few samples recorded in the target environment. In addition, forcibly sharing common initial parameters across environments allows the environment conflict issue to remain. Inspired by Learning-to-Forget (L2F) [35], we adopt an attenuation network and propose environment representations to selectively memorize target-environment-relevant components and

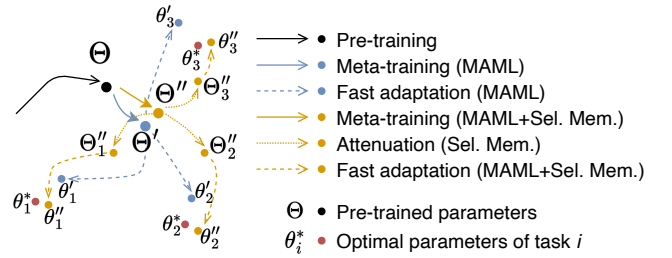


Fig. 3: An illustration of Meta-SELD++ with and without selective memory. Selective memory is proposed to tackle environment conflicts. It adds an additional step for attenuation of initial parameters before fast adaptation to the task  $i$ . The selective memory method provides a better solution (closer to the optimal solution).

selectively forget contradicting information. An illustration of our proposed environment-adaptive Meta-SELD is depicted in Fig. 3. We evaluated the proposed method on the development set of the Sony-TAU Realistic Spatial Soundscapes 2023 (STARSS23) [5] dataset and on computationally synthesized scenes. Experimental results demonstrated the effectiveness of environment-adaptive Meta-SELD.

Our main contributions can be summarized as follows:

- 1) Pre-training an environment-independent (EI) model on computationally synthesized datasets to contain as many acoustic properties as possible.
- 2) Investigating an environment adaptation approach based on Model-Agnostic Meta-Learning (MAML) and the pre-trained EI model.
- 3) Introducing a solution to selectively memorize prior information relevant to the target environment to mitigate environment conflicts.
- 4) Proposing a technique to extract environment representations for selective memory and designing comprehensive experiments to display environment representations.

## II. FAST ADAPTATION TO THE ENVIRONMENT

### A. Pre-trained environment-independent models

We train a simple convolutional recurrent neural network (CRNN) on the datasets synthesized using computationally generated SRIRs. Source code about data synthesis of spatial sound events is released<sup>1</sup>. This model is not training on samples in specific environments and is consequently termed the environment-independent (EI) model.

1) *Data synthesis*: The spatial sound event recordings are simulated by convolving monophonic sound event samples with SRIRs. The sound event samples are selected from FSD50K and AudioSet, based on the similarity of the labels in those datasets to target classes in STARSS23. These selected clips are then cleaned by the pre-trained CNN14 [39] model. We utilize CNN14 to infer these clips and select high-quality clips based on the output probability. The SRIRs are computationally generated using geometric-based methods [21], [22]. The computational generation method for SRIRs consists of two steps: microphone-array RIRs simulation and Ambisonics format converter.

We use the image source method [21] to generate microphone-array RIRs with four channels. This method replaces reflection on walls with virtual sources playing the same sound as the source and builds an RIR from the corresponding delays and attenuations. We use the python package *pyroomacoustics* [23] to simulate room acoustics. As the microphones are mounted on an acoustically hard spherical baffle in the official setup of STARSS23, the frequency response of the  $h$ -th microphone with a wave number of  $k$  on a rigid baffle of radius  $R$  for  $l$ -th image source is [40]:

$$H_{hl}(k, \psi_{hl}) = \sum_{n=0}^{\infty} i^n (2n+1) b_n(kR) P_n(\cos \psi_{hl}), \quad (1)$$

where  $\psi_{hl}$  denotes the angle between the DoA of the  $l$ -th sound source and the orientation of the  $h$ -th microphone,  $P_n$  denotes the Legendre polynomial [40]–[42],  $i$  is the imaginary unit, and  $b_n$  is the mode strength term for a rigid baffle array given by [41]

$$b_n(kR) = \frac{i}{(kR)^2 h_n^{(1)'}(kR)}, \quad (2)$$

with  $h_n^{(1)'}$  denoting the derivate of the  $n$ -th-order spherical Hankel function of the first kind [41].

The Ambisonics format conversion transforms the above-mentioned microphone-array format signals to first-order Ambisonics (FOA) format signals. The  $n$ -th-order and  $m$ -th-degree spherical harmonic function is defined with the angle  $\Psi = \{\theta, \phi\}$  as follows [41]:

$$Y_n^m(\Psi) \equiv \sqrt{\frac{2n+1}{4\pi} \frac{(n-m)!}{(n+m)!}} P_n^m(\cos \theta) e^{im\phi}, \quad (3)$$

where  $(\cdot)!$  represents the factorial operator,  $\theta$  and  $\phi$  are elevation and azimuth, and  $P_n^m(\cdot)$  is the associated Legendre function. The spherical harmonic representation of the RIRs

can be computed by using the following encoding process [17], [41]:

$$\mathbf{a}(k) = \mathbf{B}(k)^{-1} \mathbf{Y}^\dagger \mathbf{x}(k), \quad (4)$$

where

$$\mathbf{B}(k) = \begin{pmatrix} b_0 & 0 & 0 & 0 \\ 0 & b_1 & 0 & 0 \\ 0 & 0 & b_1 & 0 \\ 0 & 0 & 0 & b_1 \end{pmatrix}, \quad (5)$$

$\mathbf{x}(k)$  denotes simulated microphone-array RIR signals,  $(\cdot)^\dagger$  represents the Moore-Penrose pseudo inverse, and  $\mathbf{a}(k)$  denotes the resulting FOA format signal.  $\mathbf{Y}$  denotes first-order spherical harmony matrices with a four-channel microphone array as follows:

$$\mathbf{Y} = \begin{pmatrix} Y_0^0(\Psi_1) & Y_1^{-1}(\Psi_1) & Y_1^0(\Psi_1) & Y_1^1(\Psi_1) \\ Y_0^0(\Psi_2) & Y_1^{-1}(\Psi_2) & Y_1^0(\Psi_2) & Y_1^1(\Psi_2) \\ Y_0^0(\Psi_3) & Y_1^{-1}(\Psi_3) & Y_1^0(\Psi_3) & Y_1^1(\Psi_3) \\ Y_0^0(\Psi_4) & Y_1^{-1}(\Psi_4) & Y_1^0(\Psi_4) & Y_1^1(\Psi_4) \end{pmatrix}, \quad (6)$$

with  $\Psi_i = \{\theta_i, \phi_i\}$  being the direction of the  $i$ -th microphone.

2) *Network architecture*: Without loss of generality, in this study, we adopt a simple CRNN as our backbone for our following experiments. The CRNN is similar to the baseline of Task 3 of the DCASE 2022 Challenge [4] but with an AC-CDOA representation [10]. As shown in Fig. 4, the backbone has four convolution blocks followed by a one-layer bidirectional gated recurrent unit (BiGRU). The network takes  $C$ -channel  $T$ -frame  $F$ -mel-bin spectrograms, the concatenation of log-mel spectrograms and intensity vectors as input, and predicts active sound events of  $M$  classes with corresponding Cartesian DOA vectors for each time stamp.

### B. Meta-SELD

Given a model represented by a parameterized function  $f_\Theta$  with parameters  $\Theta$ , MAML [31] learns the initial parameters  $\Theta_0$  from general tasks  $\mathcal{T}_i$  sampled from the meta-training set  $\mathcal{D}_{\text{train}}$ . The initial parameters  $\Theta_0$  are sensitive to task-specific fine-tuning [31] and expected to perform well on unseen tasks from the meta-test set  $\mathcal{D}_{\text{test}}$  after a few parameter updates with a few task-specific samples. The task in meta-learning refers to a specific learning problem. Each task  $\mathcal{T}_i$  consists of a support set  $\mathcal{S}_i$  of  $K$  samples and a query set  $\mathcal{Q}_i$  of  $Q$  samples, analogy to the training set and test set, respectively. A new task is expected to be quickly learned with  $K$  samples, known as  $K$ -shot learning. The loss function of MAML is

$$\mathcal{L} = \sum_{\mathcal{T}_i \sim p(\mathcal{T})} \mathcal{L}_{\mathcal{T}_i}(f_\Theta), \quad (7)$$

where  $p(\mathcal{T})$ , sampled from  $\mathcal{D}_{\text{train}}$ , is a distribution over tasks that we want our model to adapt to, and  $\mathcal{L}_{\mathcal{T}_i}$  indicates the task-specific loss. In contrast to conventional supervised learning methods, the objective of which is to find optimal parameters to minimize the loss function across all training samples, MAML tries to find common generalized initial parameters across tasks and then updates the initial parameters after several iterations of training on limited data of new tasks.

<sup>1</sup><https://github.com/Jinbo-Hu/SELD-Data-Generator>

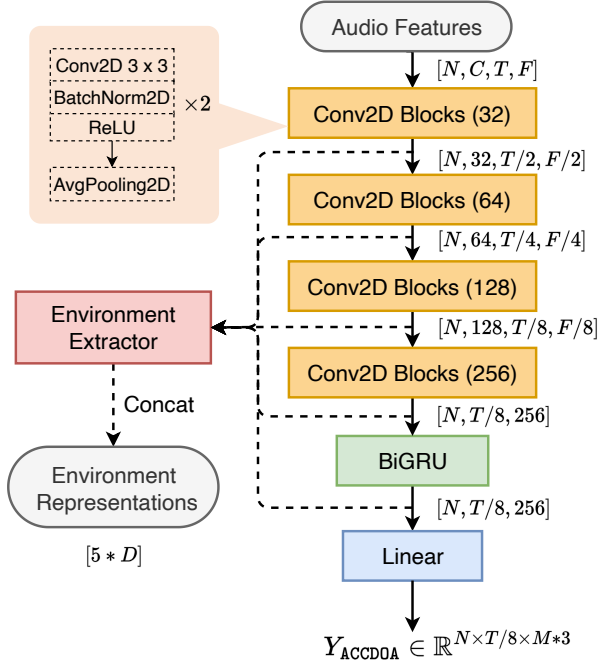


Fig. 4: The network architecture of the SELD network with the sub-network of environment representation extraction. The environment representations are extracted from output feature maps of each layer of the backbone.

There are two groups of parameters in the MAML algorithm: meta parameters and adaptation parameters. In the meta-training phase, MAML starts with randomly initialized meta parameters  $\Theta$  and then adapts to a new specific task  $\mathcal{T}_i$  with several update iterations using the support set  $\mathcal{S}_i$ . The meta parameters  $\Theta$  become adaptation parameters  $\Theta'_i$ :

$$\Theta'_i = \Theta - \alpha \nabla_{\Theta} \mathcal{L}_{\mathcal{T}_i}(f_{\Theta}, \mathcal{S}_i), \quad (8)$$

where  $\alpha$  is the adaptation learning rate. For simplicity of notation, we display only one iteration of the gradient update. After computing task-specific loss on  $\mathcal{Q}_i$  with  $f_{\Theta'_i}$  across a batch of tasks, the meta parameters are updated as follows:

$$\Theta \leftarrow \Theta - \beta \nabla_{\Theta} \sum_{\mathcal{T}_i} \mathcal{L}_{\mathcal{T}_i}(f_{\Theta'_i}, \mathcal{Q}_i), \quad (9)$$

where  $\beta$  is the meta step size. After accumulating  $\mathcal{L}_{\mathcal{T}_i}$  for several tasks,  $\Theta$  is updated by gradient descent and will be used as the initial parameters for the subsequent loops of meta-training steps.

In the meta-testing phase, a specific unseen task  $\mathcal{T}_j^{\text{test}}$  created using the meta-test set  $\mathcal{D}_{\text{test}}$  is used.  $\mathcal{T}_j^{\text{test}}$  consists of a labeled support set  $\mathcal{S}_j^{\text{test}}$  of  $K$  samples, and an unlabeled query set  $\mathcal{Q}_j^{\text{test}}$  of  $Q$  samples. We update the model, initialized by well-trained parameter  $\Theta$  in the meta-training phase, on  $\mathcal{S}_j^{\text{test}}$  to get adaptation parameters  $\Theta'_j$  using the update procedure of Eq. 8. The adaptation performance is evaluated on  $\mathcal{Q}_j^{\text{test}}$  with  $f_{\Theta'_j}$ .

We aim to adapt to an unseen environment with  $K$  samples ( $K$ -shot learning). The objective of MAML is to find optimal initial parameters across several tasks, so we need to construct

### Algorithm 1 Meta-training of proposed environment-adaptive Meta-SELD

**Require:** Distribution over all environments  $p(\mathcal{T})$ , adaptation step size  $\alpha$ , meta step size  $\beta$

**Require:** Parameters  $\Theta = \{\Theta^l\}_{l=1 \dots p}$  from pre-trained EI model, where  $l$  is the layer index and  $p$  is the number of layers of the backbone

- 1: Initialize meta parameters of backbone  $f_{\Theta}$  with the pre-trained parameters  $\Theta$ . Randomly initialize environment extractor  $g_{\Omega}$  and attenuate network  $h_{\Phi}$ .
- 2: **while** not done **do**
- 3:   Sample a batch of environments  $\mathcal{T}_i \sim p(\mathcal{T})$
- 4:   **for** each environment  $\mathcal{T}_i$  **do**
- 5:     Sample disjoint examples  $(\mathcal{S}_i, \mathcal{Q}_i)$  from  $\mathcal{T}_i$
- 6:     Compute representations of the  $i$ -th environment:  $e_i = g_{\Omega}(f_{\Theta}, \mathcal{S}_i)$
- 7:     Compute attenuation coefficients  $\lambda_i = \{\lambda_i^l\}_{l=1 \dots p}$  for each layer:  $\lambda_i = h_{\Phi}(e_i)$
- 8:     Compute attenuated initial parameters:  $\Theta_i^l = \lambda_i^l \cdot \Theta^l$
- 9:     Let  $\Theta'_i = \{\Theta_i^l\}_{l=1 \dots p}$
- 10:     **for** gradient descent step  $j := 0$  **to**  $N - 1$  **do**
- 11:       Perform gradient descent to update adaptation parameters:  $\Theta'_i \leftarrow \Theta'_i - \alpha \nabla_{\Theta'_i} \mathcal{L}_{\mathcal{T}_i}(\Theta'_i, \mathcal{S}_i)$
- 12:     **end for**
- 13:     Compute  $\mathcal{L}_{\mathcal{T}_i}(f_{\Theta'_i}, \mathcal{Q}_i)$
- 14:   **end for**
- 15:   Perform gradient descent to update meta parameters:  $\Theta \leftarrow \Theta - \beta \nabla_{\Theta} \sum_{\mathcal{T}_i} \mathcal{L}_{\mathcal{T}_i}(f_{\Theta'_i}, \mathcal{Q}_i)$
- 16:   Update  $\Omega \leftarrow \Omega - \beta \nabla_{\Omega} \sum_{\mathcal{T}_i} \mathcal{L}_{\mathcal{T}_i}(f_{\Theta'_i}, \mathcal{Q}_i)$
- 17:   Update  $\Phi \leftarrow \Phi - \beta \nabla_{\Phi} \sum_{\mathcal{T}_i} \mathcal{L}_{\mathcal{T}_i}(f_{\Theta'_i}, \mathcal{Q}_i)$
- 18: **end while**

a set of tasks from the meta-training set  $\mathcal{D}_{\text{train}}$ .  $\mathcal{D}_{\text{train}}$  is split into several tasks according to the different recording environments. Audio clips recorded in different environments belong to different tasks. We first sample a batch of environments and then sample  $K + Q$  clips in each environment, where  $K$  clips from the support set  $\mathcal{S}_i$  and  $Q$  clips from the query set  $\mathcal{Q}_i$ . The overall training procedure of MAML is summarized in Algorithm 1. Step 11 in Algorithm 1 is the inner-loop update for adaptation parameters, while Step 15 is the outer-loop update for meta parameters.

The meta-learning processes of SELD for testing and training are slightly different in the data division. Fig. 5 shows the division of the meta-training and the meta-test sets. Similar to the training, the meta-test set  $\mathcal{D}_{\text{test}}$  is partitioned based on the recording environments of each audio clip. For clips of each environment, we also chose  $K$  clips for meta-test support set  $\mathcal{S}_j^{\text{test}}$ , and all remaining clips for meta-test query set  $\mathcal{Q}_j^{\text{test}}$ . After  $N$  iterations of update on  $\mathcal{S}_j^{\text{test}}$ , the meta parameters  $\Theta$  are updated to  $\Theta'_j$ . The final performance is evaluated on  $\mathcal{Q}_j^{\text{test}}$  with  $f_{\Theta'_j}$ .

### C. Meta-SELD++

Instead of randomly initializing the meta parameters, we leverage the power of the pre-trained environment-independent

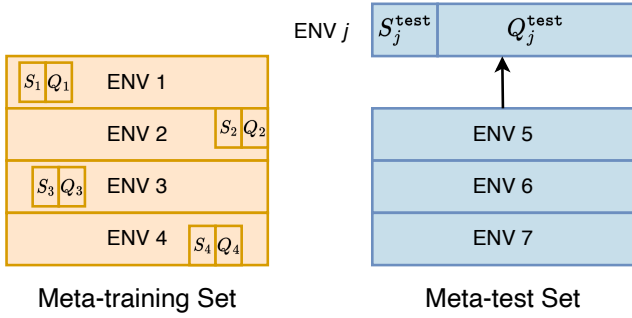


Fig. 5: The data division for the meta-training and the meta-test sets according to recording environments.

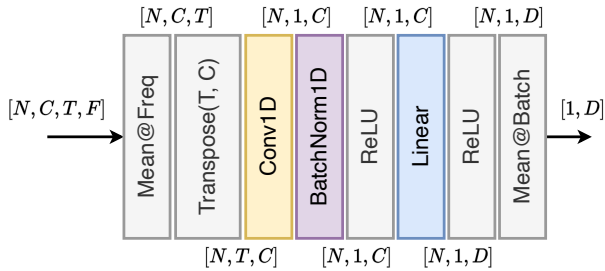


Fig. 6: A detailed implementation of the environment extractor.

(EI) model to initialize the meta parameters of MAML. In other words, we may utilize a well-trained EI model to find better initial parameters and accelerate convergence for training the meta-EI model.

Specifically, during meta-training, we initialize the meta parameters with parameters of the pre-trained EI model and then create a meta-EI model trained on synthetic datasets using collected SRIRs based on MAML. We denote this method as Meta-SELD++, whose meta parameters are initialized with pre-trained parameters. The training procedure will be expounded in Section IV-A.

### III. ENVIRONMENT-ADAPTIVE META-SELD

#### A. Selective memory

According to Eq. 7, MAML gives each task equal weight and tries to find optimal initial parameters across tasks in an average sense so that it may perform better or worse on a specific task than the conventional supervised learning method. There may be conflicts when optimizing across a batch of environments [37]. Inspired by L2F [35], which argues that forcibly sharing a common initialization in MAML induces conflicts and thus leads to the compromised location of the initialization, we selectively memorize parts relevant to the target environment. More comprehensively, we employ an environment-dependent layer-wise attenuation on the initialization, thereby dynamically controlling the influence of prior knowledge for each environment. The attenuation is generated by an attenuation network  $h_\Phi$ . Fig. 3 illustrates the optimization procedure of selective memory Meta-SELD. Compared with Meta-SELD++, selective memory adds a step to attenuate the common initial parameters for target environments before fast adaptation to corresponding environments.

One general information input to  $h_\Phi$  is gradients. At the beginning of the inner loop of MAML, task-specific gradients  $\nabla_{\Theta} \mathcal{L}_{\mathcal{T}_i}(f_{\Theta}, \mathcal{S}_i)$  on the support sets  $\mathcal{S}_i$  of the  $i$ -th environment are computed to generate layer-wise attenuation coefficients:

$$\lambda_i = h_\Phi(\nabla_{\Theta} \mathcal{L}_{\mathcal{T}_i}(f_{\Theta}, \mathcal{S}_i)), \quad (10)$$

where  $h_\Phi$  is a 3-layer MLP network with parameters  $\Phi$ , with a sigmoid in the final layer to facilitate attenuation. The layer-wise attenuation coefficients  $\lambda_i = \{\lambda_i^l\}_{l=1 \dots p}$  act on each layer of  $\Theta = \{\Theta^l\}_{l=1 \dots p}$ :

$$\Theta_i^l = \lambda_i^l \cdot \Theta^l, \quad (11)$$

where  $l$  and  $p$  indicate the layer index and the number of layers of the backbone  $f_{\Theta}$ , respectively.

Task-specific gradients generate attenuation coefficients insensitive to various environments and hence seem to be ineffective information to make attenuation environment-adaptive, which will be presented and analyzed in Section V-C. We adopt novel representations relevant to environments and expect that these representations can effectively capture and represent the acoustic properties of various environments. These representations are acquired through an unsupervised learning approach, enabling the selective memorization of target-environment-dependent prior knowledge to some extent. We denote selective memory Meta-SELD with environment representations as environment-adaptive Meta-SELD.

#### B. Environment representations

Fig. 4 depicts the method of extracting environment representations. Specifically, we employ the environment extractor to extract feature embeddings from output feature maps of each backbone layer. Subsequently, feature embeddings from each layer are concatenated to environment representations. The detail of the environment extractor is shown in Fig. 6. The feature embedding dimension  $D = 2048$  is used. The output feature maps of each layer are averaged and weighted-averaged in the batch and time dimension. We conjecture that these operators mitigate the influence of acoustic events on the feature embeddings while preserving the environmental information. Fig. 2 illustrates the environment-adaptive Meta-SELD training procedure. Step 6 in Algorithm 1 represents the extractor process of environment representations.

Our emphasis lies in evaluating the performance of Meta-SELD in unfamiliar environments. We hypothesize that audio recordings captured in diverse spatial locations within a given environment exhibit more similar acoustic properties when compared to recordings from different environments, excluding extreme cases where the speaker or microphone is close to reflections or each other. Furthermore, these acoustic properties generally remain consistent across recording moments and sound events. To test our hypothesis, we display environment representations via the similarity map and t-SNE [43] in Section V-F.

## IV. EXPERIMENTAL SETUPS

#### A. Datasets

We utilize the computationally simulated SRIRs to synthesize the datasets containing 30,000 5-second clips with rever-

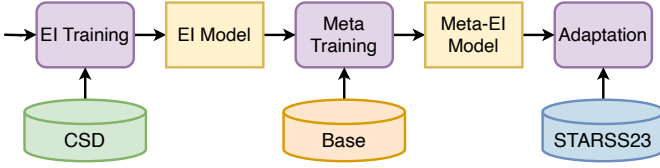


Fig. 7: A flowchart showing training procedures of our proposed method, from a randomly initialized model to the final model to adapt to unknown environments. The cylinders denote the dataset we used in different stages of the training.

beration time (RT60) from 0.3 seconds to 0.5 seconds. Sound event examples from FSD50K and AudioSet are cleaned by PANNs. We refer to the computationally simulated datasets as CSD. For simple comparison and reproducibility, we adopt the official synthetic datasets [44], which are synthesized using collected SRIRs for the baseline training of Task 3 of the DCASE Challenge in 2022 and 2023 [4], [5]. The official synthetic datasets are denoted as *Base Dataset* or *Base* in this work. The Base Dataset contains 1200 1-minute audio clips and is synthesized using real-scene SRIRs from TAU-SRIR DB [20], which are measured in 9 rooms at Tampere University. There are 16 different recording rooms in total in the development set of the STARSS23 dataset, including nine recording rooms in *dev-train-set* and seven recording rooms in *dev-test-set*. The labels of the STARSS23 evaluation set remain inaccessible, and hence all subsequent ablation experiments are based solely on the analysis of the STARSS23 development set. To further validate the effectiveness of our proposed method, we present the performance of the computationally synthesized scenes in Section V-G.

The environment-adaptive Meta-SELD involves a three-stage pipeline, each stage utilizing a distinct dataset, as illustrated in Fig. 7. We start with randomly initializing the EI model and train the EI model on CSD. Subsequently, selective memory meta-learning is applied to the EI model on the Base Dataset, served as the meta-training set  $\mathcal{D}_{\text{train}}$ , to create the meta-EI model. Finally, fast adaptation is performed to a specific environment from STARSS23 using a few samples recorded in the corresponding environment. All development sets of STARSS23 are used for meta-test set  $\mathcal{D}_{\text{test}}$  to evaluate the performance of the adaptation to unknown environments.

$\mathcal{D}_{\text{train}}$  and  $\mathcal{D}_{\text{test}}$  are divided into 9 tasks and 16 tasks, respectively, corresponding to 9 rooms and 16 rooms. In the meta-training phase, we first sample a batch of rooms and then sample a batch of examples from each room. A batch of samples from an individual room constructs a task, and a part of the samples are support samples while the remaining samples are query samples. The batch sizes of rooms and samples are set to 9 and 128, respectively. For each batch, the first 30 samples are designated as support samples in this work. In the meta-test phase, samples from each room, excluding the support samples from  $\mathcal{S}_j^{\text{test}}$ , comprise the final test (query) set  $\mathcal{Q}_j^{\text{test}}$ . We will evaluate the performance of parameterized function  $f_{\Theta'_j}$  with adaptation parameters  $\Theta'_j$  on  $\mathcal{Q}_j^{\text{test}}$  after iteration updates on  $\mathcal{S}_j^{\text{test}}$  with the initial parameters  $\Theta$ .

TABLE I: Results of the computationally synthesized datasets. Methods are evaluated on all development sets of STARSS23.

Dataset	ER <sub>20°</sub> ↓	F <sub>20°</sub> ↑	LE <sub>CD</sub> ↓	LR <sub>CD</sub> ↑	ε <sub>SELD</sub> ↓
Base	0.722	<b>23.2%</b>	<b>22.2°</b>	39.5%	0.555
CSD	0.746	20.9%	25.6°	41.4%	0.566
Base + CSD	<b>0.697</b>	23.1%	22.6°	<b>44.3%</b>	<b>0.537</b>

### B. Evaluation metrics

We use a joint metric of localization and detection [45], [46] here: two location-dependent detection metrics, F-score ( $F_{\leq 20^\circ}$ ) and error rate ( $ER_{\leq 20^\circ}$ ), and two class-dependent localization metrics, localization recall ( $LR_{CD}$ ) and localization error ( $LE_{CD}$ ).  $F_{\leq 20^\circ}$  and  $ER_{\leq 20^\circ}$  consider true positives predicted within a spatial threshold  $20^\circ$  away from the ground truth.  $LE_{CD}$  and  $LR_{CD}$  compute the mean angular error and true positive rate in the case when the types of sound events are predicted correctly, respectively.

We use an aggregated SELD metric for the method comparison and hyper-parameter selection:

$$\mathcal{E}_{\text{SELD}} = \frac{1}{4} [ER_{\leq 20^\circ} + (1 - F_{\leq 20^\circ}) + \frac{LE_{CD}}{180^\circ} + (1 - LR_{CD})]. \quad (12)$$

A macro-average of  $F_{\leq 20^\circ}$ ,  $LR_{CD}$ ,  $LE_{CD}$ , and  $\mathcal{E}_{\text{SELD}}$  across classes is used. A good system should have small  $ER_{\leq 20^\circ}$ , large  $F_{\leq 20^\circ}$ , small  $LE_{CD}$ , large  $LR_{CD}$ , and small  $\mathcal{E}_{\text{SELD}}$ . Note that different from [37], where room-wise metrics are micro-averaged in the end, we compute the metrics in each room and then macro-average the metrics across rooms.

### C. Hyper-parameters

The sampling rate is 24 kHz. We extract 64-dimensional log mel spectrograms from four-channel FOA signals with a Hanning window of 1024 points, and a hop size of 320. Each audio clip is segmented to a fixed length of five seconds with no overlap for training and inference.

AdamW [47] is used to update meta parameters, while SGD is used to update adaptation parameters. The batch size is 128. For training the conventional supervised learning models, the learning rate is set to 0.001 for the first 60 epochs out of 80 epochs and is then decreased by 10% every 10 epochs. In the meta-training phase, we find that setting the momentum to 0.01 in the Batch Normalization layer [48] has better performance. We set one epoch containing nine meta batches, which encompass all rooms within the Base Dataset. Subsequently, the gradients of one epoch are averaged to update meta parameters in the outer loop step. For training Meta-SELD++, the learning rate is 0.0003 for the first 300 epochs out of 500 epochs and is then decreased by 10% every 100 epochs. We only consider 5 iteration updates in the inner loop of MAML. All networks are implemented using PyTorch.

## V. EXPERIMENTS

### A. Effect of synthetic data

We evaluate our synthetic data using the conventional supervised learning method. The model is trained on the Base Dataset (Base) and CSD, and then evaluated on all development sets of STARSS23.

TABLE II: Description of utilized models. (·) denotes the dataset for training.  $\mathcal{S}_j^{\text{test}}$  indicates the support set from the  $j$ -th room of STARSS23.

Approach	Initial parameters	Datasets
<b>Conventional supervised learning methods</b>		
SELD (·)	-	The combinations of Base, CSD, and $\mathcal{S}_j^{\text{test}}$
SELD (·) w/ adapt. or Fine-tuned SELD	SELD (Base) or SELD (Base + CSD)	$\mathcal{S}_j^{\text{test}}$
<b>Meta learning methods</b>		
Meta-SELD	-	Base $\mathcal{S}_j^{\text{test}}$
Meta-SELD w/ adapt.	Meta-SELD	Base $\mathcal{S}_j^{\text{test}}$
Meta-SELD++	SELD (CSD)	Base $\mathcal{S}_j^{\text{test}}$
Meta-SELD++ w/ adapt.	Meta-SELD++	$\mathcal{S}_j^{\text{test}}$
Sel. Mem. Meta-SELD	SELD (CSD)	Base $\mathcal{S}_j^{\text{test}}$
Sel. Mem. Meta-SELD w/ adapt.	Sel. Mem. Meta-SELD	$\mathcal{S}_j^{\text{test}}$

Table I shows the results of the data synthesis method. The results demonstrate that the model trained on the CSD can generalize to real-scene datasets. Comparing Base with CSD, we observe the performance gap is mainly in localization. One of the possible reasons is that there is some discrepancy between computationally simulated SRIRs and measured SRIRs in real scenes. In addition, adding CSD to the Base Dataset for training further improves the performance.

### B. Effect of Meta-SELD

To demonstrate the effectiveness of our proposed Meta-SELD, we compare the Meta-SELD, the SELD method, and the fine-tuned SELD method. The differences among these methods are described in Table II. Macro-averaged metrics for all 16 rooms of STARSS23 are shown in Table III. In SELD (Base +  $\mathcal{S}_j^{\text{test}}$ ), the support set  $\mathcal{S}_j^{\text{test}}$  from the  $j$ -th room of STARSS23 is added to the synthetic datasets for training from scratch, and the query set  $\mathcal{Q}_j^{\text{test}}$  is used for evaluating that specific model. This approach, however, requires training multiple models from scratch, one for each specific room of STARSS23. In SELD (Base), we first train an EI model on the Base Dataset and then fine-tune (adapt) on  $\mathcal{S}_j^{\text{test}}$ . In Meta-SELD, we apply MAML to a SELD model with random initialized meta-parameters. The SELD (Base) and Meta-SELD methods without adaptation refer to no fine-tuning on  $\mathcal{S}_j^{\text{test}}$ .

The top block of Table III presents the method using the Base Dataset for training or meta-training, while the bottom block presents the method using the Base Dataset and computationally simulated datasets. In terms of the average performance, we can see that after adaptation on  $\mathcal{S}_j^{\text{test}}$ , both Meta-SELD and Meta-SELD++ exhibit superior performance in comparison to the corresponding fine-tuned SELD method. In a comparison between SELD (Base) and Meta-SELD, we observe a bigger performance gap in Meta-SELD with and without adaptation, which means the meta parameters of Meta-SELD are more suitable for adapting to a new environment. However, the performance gap in Meta-SELD++ becomes smaller and meta parameters from Meta-SELD++ outperform parameters from SELD (Base + CSD). We conjecture the phenomenon results from conflicts while optimizing among environments, especially obvious in Meta-SELD++. The SELD

TABLE III: The performance of meta-learning-based and conventional supervised-learning-based methods. All of the methods are evaluated on  $\mathcal{Q}_i^{\text{test}}$  from STARSS23.

Method	Adapt.	ER <sub>20°</sub> ↓	F <sub>20°</sub> ↑	LE <sub>CD</sub> ↓	LR <sub>CD</sub> ↑	$\mathcal{E}_{\text{SELD}}$ ↓
SELD (Base + $\mathcal{S}_i^{\text{test}}$ )	-	0.642	32.8%	21.1°	54.5%	0.471
SELD (Base)	✗	0.742	30.1%	23.9°	53.6%	0.509
	✓	0.690	31.6%	22.8°	53.7%	0.491
Meta-SELD	✗	0.718	29.8%	24.0°	53.5%	0.504
	✓	0.639	32.6%	21.3°	52.8%	0.476
SELD (Base + CSD + $\mathcal{S}_i^{\text{test}}$ )	-	0.653	33.6%	22.6°	58.2%	0.465
SELD (Base + CSD)	✗	0.714	28.6%	25.2°	58.8%	0.495
	✓	0.686	30.1%	24.7°	59.2%	0.482
Meta-SELD++	✗	0.698	30.5%	23.6°	59.6%	0.482
	✓	0.657	31.4%	23.2°	59.0%	0.470

TABLE IV: Ablation studies on types of input in selective memory Meta-SELD.

Method	Input	ER <sub>20°</sub> ↓	F <sub>20°</sub> ↑	LE <sub>CD</sub> ↓	LR <sub>CD</sub> ↑	$\mathcal{E}_{\text{SELD}}$ ↓
Meta-SELD++ w/ adapt.	-	0.657	31.4%	23.2°	59.0%	0.470
+ Selective Memory	None	0.635	33.4%	21.5°	60.2%	0.455
	Gradients	0.635	34.2%	21.6°	57.4%	0.460
	Rep. (Ours)	0.629	34.1%	21.7°	59.6%	0.453

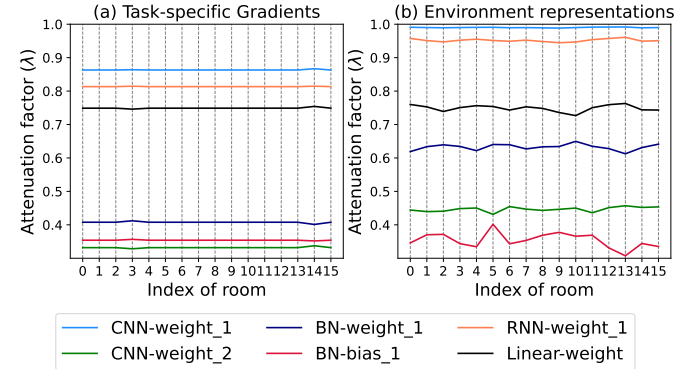


Fig. 8: Generated room-and-layer-wise attenuation factors  $\lambda$  using selective memory for each room of STARSS23.

method, which adds the support set  $\mathcal{S}_j^{\text{test}}$  for training, performs the best among these methods. This phenomenon may be attributed to the fact that training multiple independent models from scratch could avoid compromise in these environments.

### C. Effect of selective memory

1) *Inputs to selective memory*: Table IV shows the results of three types of input in the selective memory methods, the task-specific gradients on the support set  $\mathcal{S}_i$ , "None", and the environment representations. The input "None" in the selective memory method refers to layer-wise learnable parameters as attenuation coefficients instead of being generated by the attenuation network. We see that applying selective memory to Meta-SELD++ obtains performance improvement, particularly in localization. These methods are even more effective than the SELD (Base + CSD +  $\mathcal{S}_i^{\text{test}}$ ) in Table III. Among these types of inputs, the environment representations perform better. This



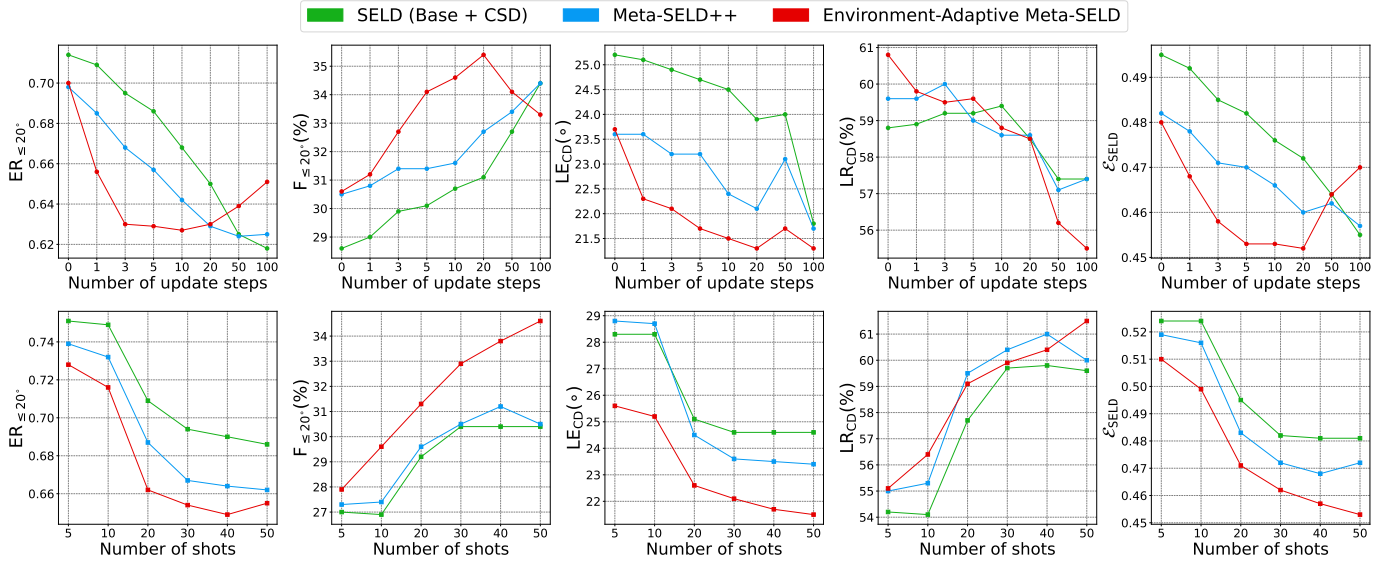


Fig. 9: The effect of hyper-parameters of MAML. Each column represents one metric. **Top row**: The number of inner-loop update steps. **Bottom row**: The number of support samples.

TABLE V: Ablation studies on approaches for extracting environment representations.

Approach	ER <sub>20°</sub> ↓	F <sub>20°</sub> ↑	LE <sub>CD</sub> ↓	LR <sub>CD</sub> ↑	ε <sub>SELD</sub> ↓
Last emb. (Mean)	0.660	33.1%	21.7°	59.1%	0.465
Last emb. (Encode)	0.635	33.8%	<b>21.2°</b>	58.4%	0.458
Env. rep. (Ours)	<b>0.629</b>	<b>34.1%</b>	21.7°	<b>59.6%</b>	<b>0.453</b>

exhibits the effectiveness of environment representations as the input to the selective memory method.

2) *Attenuation factors*: Fig. 8 illustrates the attenuation factor  $\lambda$  of a few typical layers for each room of STARSS23. However, observing room-and-layer-wise attenuation factor  $\lambda$  derived from the task-specific gradients, we note that  $\lambda$  varies over a small range from room to room. This suggests that  $\lambda$  can not be adaptive to the diverse acoustic environments of these rooms. We analyze the inputs to the attenuation network, task-specific gradients on  $S_i$ , and find that most gradients exhibit diminutive magnitudes. This phenomenon can be attributed to the pre-trained EI model, which initializes the meta-parameters of Meta-SELD++, resulting in minute gradient values. In contrast, a comparison of the gradients and representations as input to the attenuation network indicates that environment representations generate more environment-adaptive attenuation factors  $\lambda$ . The changes in these attenuation factors are more conspicuous from room to room.

For CNN-weight\_1 in Fig. 8, which is the first layer of the backbone, we observe that generated  $\lambda$  of this layer is relatively large and changes pretty little among rooms, compared with subsequent layers. The initial layers encode environment-independent features, while deep layers prefer environment-adaptive attenuation and encode environment-dependent features, which aligns with the observation of [35].

3) *Representations of Environments*: We investigate various techniques for extracting environment representations: feature maps from the last layer (before the linear layer) that are aver-

aged in the batch and time axes, feature embeddings derived from the last layer, and environment representations constituted by concatenated feature embeddings from all preceding layers. Table V demonstrates the effectiveness of the environment extractor and preceding feature embeddings. Feature maps from the last layer encoded by the environment extractor perform better compared to being directly averaged. Moreover, preceding feature embeddings provide more information and further performance improvement.

#### D. Effect of adaptation setups

The most important hyper-parameters in the adaptation phase of MAML include the number of inner-loop update steps and support samples. Intuitively, the inner-loop optimization should be consistent during meta-training and meta-testing. However, the large number of update steps and support samples leads to excessive computation and memory burdens. We exploit previously well-trained parameters and investigate the effect of adaptation setups in meta-testing.

The top row of Fig. 9 shows the effect of the number of update steps on the adaptation of SELD (Base + CSD), Meta-SELD++, and environment-adaptive Meta-SELD. The environment-adaptive Meta-SELD achieves more efficient adaptation. The benefits come from selectively memorizing necessary information, helping the learner adapt to new environments more quickly.

We also investigate the effect of the number of shots (support samples). Note that in this experimental setup, we select the first 50 samples of each room as the support set, and all remaining samples are as the query set. The bottom row of Fig. 9 shows that meta-learning-based methods exploit support samples more effectively. When the number of support samples increases in the environment-adaptive Meta-SELD method, the performance is consistently improved, but the magnitude of performance improvement also appears to decrease.

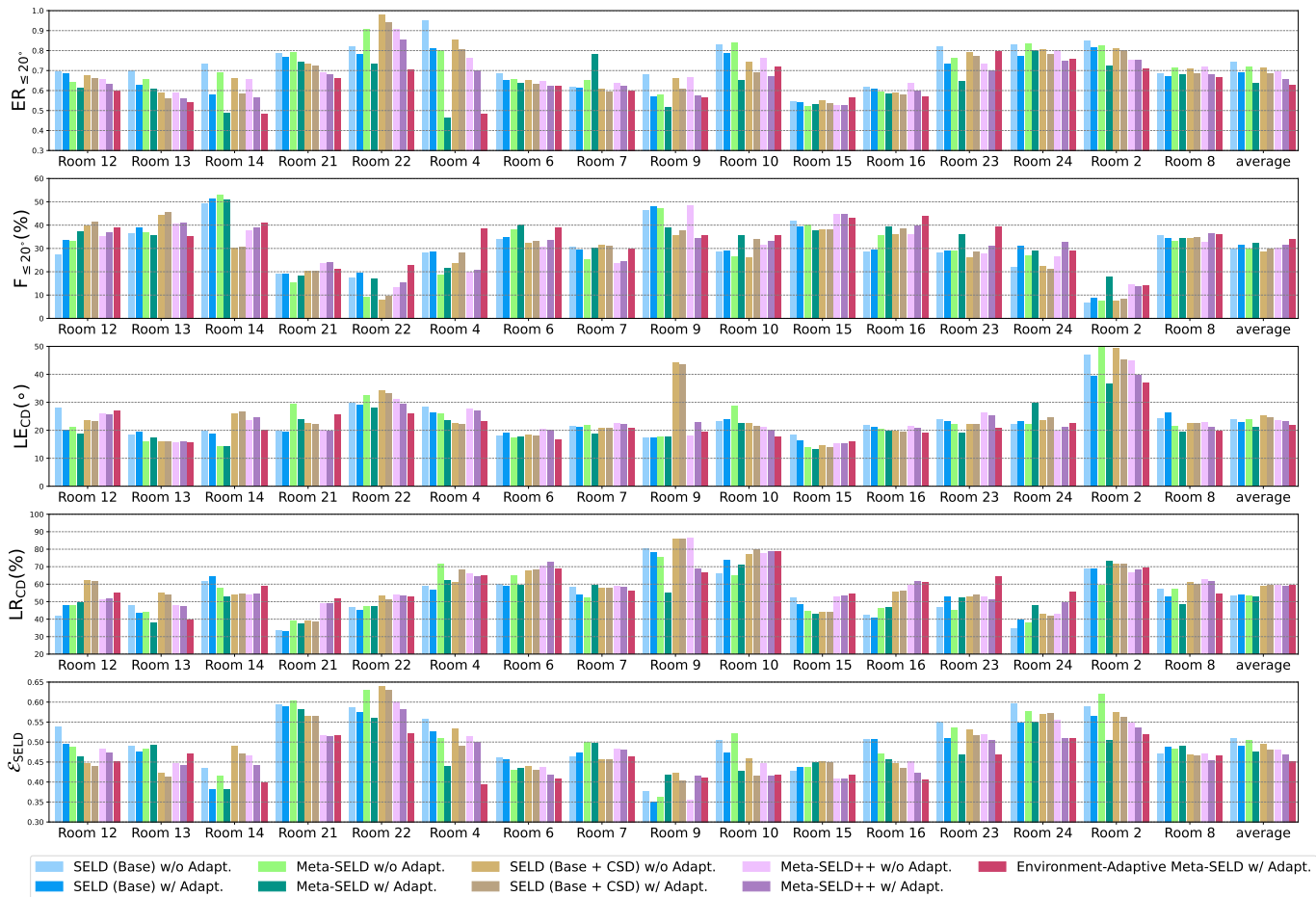


Fig. 10: Room-wise performance of all development sets of STARSS23. All methods are evaluated on  $Q_j^{\text{test}}$ . Note that the *average* score of each metric computes the macro-average performance of all these rooms.

### E. Room-wise performance

Fig. 10 shows the room-wise metrics. Through a comparative analysis of conventional supervised-learning-based and meta-learning-based methods on identical datasets, we observe that meta-learning-based methods can reduce  $\mathcal{E}_{\text{SELD}}$  effectively in rooms where conventional supervised-learning-based methods exhibit high  $\mathcal{E}_{\text{SELD}}$ , such as Room 2, Room 4, and Room 22. This means when a model has an unsatisfactory generalization to a specific room below the average performance, using a few samples collected in the specific room for adapting could improve the performance significantly. However, we also observe performance degradation or insignificant improvement in  $\mathcal{E}_{\text{SELD}}$ , even though some new samples of unseen environments are used for adapting in both conventional supervised-learning-based and meta-learning-based methods, for example, in Room 7 and Room 15. This phenomenon could arise from the fact that our methods have difficulty extracting valid information for training from new samples. In Room 9, the performance of SELD (Base) and SELD (Base + CSD) is improved after fine-tuning using some new samples of the corresponding room, but the performance of Meta-SELD and Meta-SELD++ after adaptation is degraded. The reason may be that compromised initial meta parameters among those rooms fail to adapt to the environment. The meta-learning-based methods find general initial

parameters that can be adapted to unknown environments in the sense of average, and experimental results demonstrate that meta-learning-based methods outperform the conventional supervised-learning-based methods in most rooms and perform better on average.

In contrast to SELD (Base + CSD), the environment-adaptive Meta-SELD exhibits comparable average performance in  $\text{LR}_{\text{CD}}$ , but lower  $\text{LE}_{\text{CD}}$ . Consequently, performance improvement in localization is the main factor for the reduction in  $\mathcal{E}_{\text{SELD}}$ . Additionally, the performance improvement in Room 2 and Room 22 can also be attributed to analogous factors.

### F. Environment representations

To interpret the representation extracted by the sub-network in Fig. 4, we study the relationship between the representation and the environment. We hypothesize that different clips recorded at various spatial positions in the same environment generally have more similar acoustic properties in contrast to various environments, except in extreme cases. Therefore, we extract representations from several disjoint batches of samples, and then we compute the similarity between the representations and visualize these representations via t-SNE [43]. Fig. 11 shows the visualization of extracted representations.

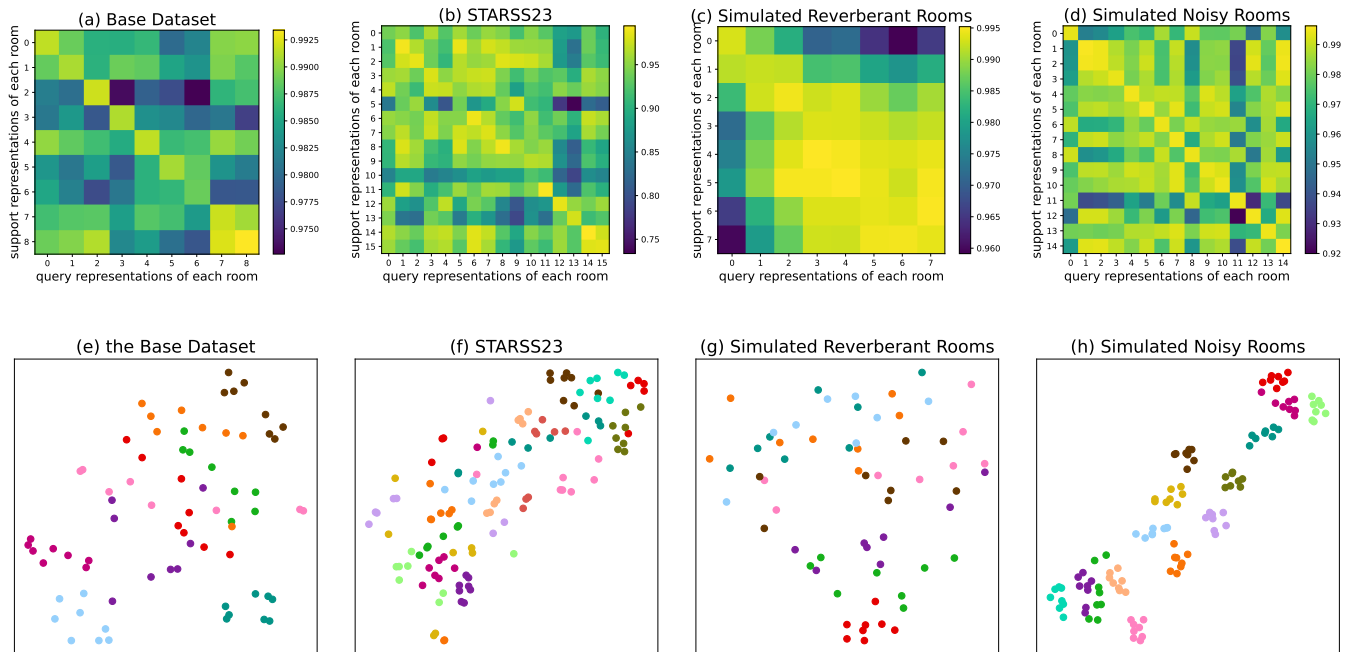


Fig. 11: Visualization of environment representations. The four plots (a-d) of the top row display the cosine similarity maps between support representations and query representations. The four plots (e-h) of the bottom row display the representations via t-SNE, and points of the same color indicate representations from the same room. Four datasets are shown: the Base Dataset, the development set of STARSS23, computationally simulated reverberant rooms, and computationally simulated noisy rooms.

The SELD performance is greatly affected by noise and reverberation. To dynamically control the acoustic properties of environments to investigate the representation, we also simulate both reverberant rooms and noisy rooms. For the reverberant simulations, rooms of the same size are simulated at intervals of 0.3-second RT60, ranging from 0.4 to 2.5 seconds, therefore, there are 8 rooms with different RT60 in total. For the noisy simulations, we simulate 15 rooms of the same size, absorption coefficients, and reflection orders. Subsequently, we add ambient noise from the NoiseX-92 [49] database into synthetic recordings to generate SNR ranging from 10 dB to 15 dB. The NoiseX-92 database contains 15 types of ambient noise. Hence each room has a unique noise type. All sound event examples for synthesizing are randomly sampled from FSD50K and AudioSet. Based on the previously trained model using the environment-adaptive Meta-SELD method, we directly perform an inference (meta-test) on these simulated datasets.

1) *Similarity Maps*: Representations from the same or similar rooms should have a high similarity. In this work, the cosine distance of two representations is used to measure their similarity. For a batch of 128 samples from the same room, we extract support representations from the first 30 samples, corresponding to the number of support samples for adaptation, and query representations from the last 98 samples. The cosine similarity is computed between support representations from a room and query representations from the same or other rooms.

Fig. 11 (a) and (b) present the cosine similarity maps on

the Base Dataset and STARSS23. The experimental results show that all diagonal elements are the maximum of their rows of the similarity matrix on the Base Dataset, while 12/16 of diagonal elements are the maximum of their rows on STARSS23. Fig. 11(c) and (d) show the cosine similarity maps on the simulated reverberant rooms and simulated noisy rooms. We see that these maps are relatively symmetrical. The diagonal elements of the similarity matrix are pretty large. In addition, we observe environment representations have a high resolution in rooms with low RT60, but a low resolution in rooms with high RT60. The differences in the environment representations of these rooms with high RT60 are small. This may result from the small range RT60 of the training set.

2) *Visualization of representations via t-SNE*: We sample 8 batches of clips from each dataset, with 32 clips per batch, and then compute representations for each batch<sup>2</sup>. Empirically, we find the learned representations cluster meaningfully: representations from the same room tend to be clustered, as shown in Fig. 11 (e-h). Especially in Fig. 11(h), different recordings with the same noisy type have similar features, which leads to better clustering performance.

These observations demonstrate the extracted representations are relevant to the environments.

### G. Results on computationally synthesized scenes

We evaluate the method on computationally synthesized scenes to further validate the effectiveness of environment-

<sup>2</sup>For STARSS23, the number of clips is less than 256 in a few rooms, therefore, we repeat the corresponding batch of clips along the batch dimension.

TABLE VI: The performance of proposed methods on computationally synthesized scenes.

Method	Adapt.	ER <sub>20°</sub> ↓	F <sub>20°</sub> ↑	LE <sub>CD</sub> ↓	LR <sub>CD</sub> ↑	ε <sub>SELD</sub> ↓
SELD (Base + CSD)	✗	0.739	15.0%	30.0°	30.8%	0.612
	✓	0.733	15.4%	28.9°	30.6%	0.609
Meta-SELD++	✗	0.772	13.9%	32.1°	<b>32.0%</b>	0.623
	✓	0.745	15.5%	30.4°	31.8%	0.610
Environment-Adaptive Meta-SELD (Ours)	✓	<b>0.692</b>	<b>17.6%</b>	<b>25.3°</b>	31.3%	<b>0.586</b>

adaptive Meta-SELD. These scenes are represented as semantically labeled 3D meshes from the 3D-FRONT dataset [50], which contains 18,968 diversely furnished rooms in 6,813 professionally designed houses. We computationally simulate SRIRs of 15 houses sampled from the 3D-FRONT dataset, which is the same as the simulation of the Geometric-Wave Acoustic (GWA) dataset [51]. We synthesize 256 5-second spatial recordings for each acoustic environment with these simulated SRIRs and sound events from FSD50K [18] and AudioSet [19]. Ambient noise from the NoiseX-92 [49] database is also mixed into spatial recordings to generate signal-to-noise (SNR) ranging from 10 dB to 15 dB.

We leverage the previous methods trained on CSD and Base Dataset to perform an inference (meta-test) on the simulated dataset. Table VI presents the results on computationally synthesized scenes. Notably, we see weak generalizations to these environments for both conventional supervised learning and meta-learning methods, due to disparities in environmental conditions between the training and test datasets. Additionally, the considerable variation in distribution between meta-training sets and meta-testing sets puts the meta-learned prior knowledge at high risk of losing effectiveness [29], [52], [53]. However, the incorporation of selective memory into Meta-SELD++ manifests superior performance in contrast to other methods, particularly improving the localization performance.

## VI. CONCLUSION

This study presents environment-adaptive Meta-SELD designed for efficient adaptation to specific acoustic environments using a limited number of samples recorded in those settings. We apply Model-Agnostic Meta-Learning (MAML) to a pre-trained environment-independent SELD model to obtain generalized initial parameters for different environments. Subsequently, we introduce selective memory and environment representations in Meta-SELD++ to alleviate conflicts and the limitations of common initialization across different environments. When evaluated on the development set of the STARSS23 datasets and computationally synthesized scenes, our proposed environment-adaptive Meta-SELD demonstrates superior performance compared to conventional supervised-learning-based SELD methods. Furthermore, we investigate and exhibit environment representations. Experimental results show that environment representations effectively capture the nuances of diverse acoustic environments. The potential applications of these environment representations are extensive, promising significant advancements in enhancing acoustic scene analysis in diverse settings.

## REFERENCES

- [1] S. Adavanne, A. Politis, and T. Virtanen, "A multi-room reverberant dataset for sound event localization and detection," in *Proceedings of Detection and Classification of Acoustic Scenes and Events (DCASE) Workshop*, 2019, pp. 10–14.
- [2] A. Politis, S. Adavanne, and T. Virtanen, "A dataset of reverberant spatial sound scenes with moving sources for sound event localization and detection," in *Proceedings of Detection and Classification of Acoustic Scenes and Events (DCASE) Workshop*, 2020, pp. 165–169.
- [3] A. Politis, S. Adavanne, D. Krause, A. Deleforge, P. Srivastava, and T. Virtanen, "A dataset of dynamic reverberant sound scenes with directional interferers for sound event localization and detection," in *Proceedings of Detection and Classification of Acoustic Scenes and Events (DCASE) Workshop*, 2021, pp. 125–129.
- [4] A. Politis, K. Shimada, P. Sudarsanam, S. Adavanne, D. Krause, Y. Koyama, N. Takahashi, S. Takahashi, Y. Mitsufuji, and T. Virtanen, "STARSS22: A dataset of spatial recordings of real scenes with spatiotemporal annotations of sound events," in *Proceedings of Detection and Classification of Acoustic Scenes and Events (DCASE) Workshop*, 2022, pp. 161–165.
- [5] K. Shimada, A. Politis, P. Sudarsanam, D. Krause, K. Uchida, S. Adavanne, A. Hakala, Y. Koyama, N. Takahashi, S. Takahashi, T. Virtanen, and Y. Mitsufuji, "STARSS23: An audio-visual dataset of spatial recordings of real scenes with spatiotemporal annotations of sound events," *arXiv preprint arXiv: 2306.09126*, 2023.
- [6] S. Adavanne, A. Politis, J. Nikunen, and T. Virtanen, "Sound event localization and detection of overlapping sources using convolutional recurrent neural networks," *IEEE Journal of Selected Topics in Signal Processing*, vol. 13, no. 1, pp. 34–48, 2019.
- [7] Y. Cao, T. Iqbal, Q. Kong, Y. Zhong, W. Wang, and M. D. Plumbley, "Event-independent network for polyphonic sound event localization and detection," in *Proceedings of Detection and Classification of Acoustic Scenes and Events (DCASE) Workshop*, 2020, pp. 11–15.
- [8] Y. Cao, T. Iqbal, Q. Kong, F. An, W. Wang, and M. D. Plumbley, "An improved event-independent network for polyphonic sound event localization and detection," in *Proceedings of IEEE International Conference on Acoustics, Speech and Signal Processing (ICASSP)*, 2021, pp. 885–889.
- [9] J. Hu, Y. Cao, M. Wu, Q. Kong, F. Yang, M. D. Plumbley, and J. Yang, "A track-wise ensemble event independent network for polyphonic sound event localization and detection," in *Proceedings of IEEE International Conference on Acoustics, Speech and Signal Processing (ICASSP)*, 2022, pp. 9196–9200.
- [10] K. Shimada, Y. Koyama, N. Takahashi, S. Takahashi, and Y. Mitsufuji, "ACCDOA: Activity-coupled cartesian direction of arrival representation for sound event localization and detection," in *Proceedings of IEEE International Conference on Acoustics, Speech and Signal Processing (ICASSP)*, 2021, pp. 915–919.
- [11] K. Shimada, Y. Koyama, S. Takahashi, N. Takahashi, E. Tsunoo, and Y. Mitsufuji, "Multi-ACCDOA: Localizing and detecting overlapping sounds from the same class with auxiliary duplicating permutation invariant training," in *Proceedings of IEEE International Conference on Acoustics, Speech and Signal Processing (ICASSP)*, 2022, pp. 316–320.
- [12] M. Wang and W. Deng, "Deep visual domain adaptation: A survey," *Neurocomputing*, vol. 312, pp. 135–153, 2018.
- [13] W. M. Kou and M. Loog, "A review of domain adaptation without target labels," *IEEE Transactions on Pattern Analysis and Machine Intelligence*, vol. 43, no. 3, pp. 766–785, 2019.
- [14] J. Hu, Y. Cao, M. Wu, Q. Kong, F. Yang, M. D. Plumbley, and J. Yang, "Sound event localization and detection for real spatial sound scenes: Event-independent network and data augmentation chains," in *Proceedings of Detection and Classification of Acoustic Scenes and Events (DCASE) Workshop*, 2022, pp. 46–50.
- [15] P.-A. Grumiaux, S. Kitić, L. Girin, and A. Guérin, "A survey of sound source localization with deep learning methods," *The Journal of the Acoustical Society of America*, vol. 152, no. 1, pp. 107–151, 2022.
- [16] Q. Wang, J. Du, H. Wu, J. Pan, F. Ma, and C. Lee, "A four-stage data augmentation approach to ResNet-Convformer based acoustic modeling for sound event localization and detection," *IEEE/ACM Transactions on Audio, Speech, and Language Processing*, vol. 31, pp. 1251–1264, 2023.
- [17] Y. Koyama, K. Shigemitsu, M. Takahashi, K. Shimada, N. Takahashi, E. Tsunoo, S. Takahashi, and Y. Mitsufuji, "Spatial data augmentation with simulated room impulse responses for sound event localization and detection," in *Proceedings of IEEE International Conference on Acoustics, Speech and Signal Processing (ICASSP)*, 2022, pp. 8872–8876.

- [18] E. Fonseca, X. Favory, J. Pons, F. Font, and X. Serra, "FSD50K: An open dataset of human-labeled sound events," *IEEE/ACM Transactions on Audio, Speech, and Language Processing*, vol. 30, pp. 829–852, 2022.
- [19] J. F. Gemmeke, D. P. Ellis, D. Freedman, A. Jansen, W. Lawrence, R. C. Moore, M. Plakal, and M. Ritter, "Audio Set: An ontology and human-labeled dataset for audio events," in *Proceedings of IEEE International Conference on Acoustics, Speech and Signal Processing (ICASSP)*, 2017, pp. 776–780.
- [20] A. Politis, S. Adavanne, and T. Virtanen, "TAU Spatial Room Impulse Response Database (TAU-SRIR DB)," Apr. 2022. [Online]. Available: <https://doi.org/10.5281/zenodo.6408611>
- [21] J. B. Allen and D. A. Berkley, "Image method for efficiently simulating small-room acoustics," *The Journal of the Acoustical Society of America*, vol. 65, no. 4, pp. 943–950, 1979.
- [22] Z. Tang, L. Chen, B. Wu, D. Yu, and D. Manocha, "Improving reverberant speech training using diffuse acoustic simulation," in *Proceedings of IEEE International Conference on Acoustics, Speech and Signal Processing (ICASSP)*. IEEE, 2020, pp. 6969–6973.
- [23] R. Scheibler, E. Bezzam, and I. Dokmanić, "Pyroomacoustics: A python package for audio room simulation and array processing algorithms," in *Proceedings of IEEE International Conference on Acoustics, Speech and Signal Processing (ICASSP)*, 2018, pp. 351–355.
- [24] D. Diaz-Guerra, A. Miguel, and J. R. Beltran, "gpuRIR: A python library for room impulse response simulation with GPU acceleration," *Multimedia Tools and Applications*, vol. 80, pp. 5653–5671, 2021.
- [25] D. P. Jarrett, E. A. Habets, M. R. Thomas, and P. A. Naylor, "Rigid sphere room impulse response simulation: Algorithm and applications," *The Journal of the Acoustical Society of America*, vol. 132, no. 3, pp. 1462–1472, 2012.
- [26] F. Zhuang, Z. Qi, K. Duan, D. Xi, Y. Zhu, H. Zhu, H. Xiong, and Q. He, "A comprehensive survey on transfer learning," *Proceedings of the IEEE*, vol. 109, no. 1, pp. 43–76, 2020.
- [27] Y. Wang, Q. Yao, J. T. Kwok, and L. M. Ni, "Generalizing from a few examples: A survey on few-shot learning," *ACM Computing Surveys*, vol. 53, no. 3, pp. 1–34, 2020.
- [28] T. Hospedales, A. Antoniou, P. Micaelli, and A. Storkey, "Meta-learning in neural networks: A survey," *IEEE Transactions on Pattern Analysis and Machine Intelligence*, vol. 44, no. 9, pp. 5149–5169, 2021.
- [29] W.-Y. Chen, Y.-C. Liu, Z. Kira, Y.-C. F. Wang, and J.-B. Huang, "A closer look at few-shot classification," in *Proceedings of International Conference on Learning Representations (ICLR)*, 2019.
- [30] N. Gao, H. Ziesche, N. A. Vien, M. Volpp, and G. Neumann, "What matters for meta-learning vision regression tasks?" in *Proceedings of IEEE/CVF Conference on Computer Vision and Pattern Recognition (CVPR)*, 2022, pp. 14 776–14 786.
- [31] C. Finn, P. Abbeel, and S. Levine, "Model-agnostic meta-learning for fast adaptation of deep networks," in *Proceedings of International Conference on Machine Learning (ICML)*, 2017, pp. 1126–1135.
- [32] S.-F. Huang, C.-J. Lin, D.-R. Liu, Y.-C. Chen, and H.-y. Lee, "Meta-TTS: Meta-learning for few-shot speaker adaptive text-to-speech," *IEEE/ACM Transactions on Audio, Speech, and Language Processing*, vol. 30, pp. 1558–1571, 2022.
- [33] M. Barhoush, A. Hallawa, A. Peine, L. Martin, and A. Schmeink, "Localization-driven speech enhancement in noisy multi-speaker hospital environments using deep learning and meta learning," *IEEE/ACM Transactions on Audio, Speech, and Language Processing*, vol. 31, pp. 670–683, 2023.
- [34] W. Lin and M.-W. Mak, "Model-agnostic meta-learning for fast text-dependent speaker embedding adaptation," *IEEE/ACM Transactions on Audio, Speech, and Language Processing*, vol. 31, pp. 1866–1876, 2023.
- [35] S. Baik, S. Hong, and K. M. Lee, "Learning to forget for meta-learning," in *Proceedings of IEEE/CVF Conference on Computer Vision and Pattern Recognition (CVPR)*, 2020, pp. 2379–2387.
- [36] R. Vuorio, S.-H. Sun, H. Hu, and J. J. Lim, "Multimodal model-agnostic meta-learning via task-aware modulation," in *Proceedings of Advances in Neural Information Processing Systems (NeurIPS)*, vol. 32, 2019.
- [37] J. Hu, Y. Cao, M. Wu, Z. Yu, F. Yang, W. Wang, M. D. Plumbley, and J. Yang, "Meta-SELD: Meta-learning for fast adaptation to the new environment in sound event localization and detection," in *Proceedings of Detection and Classification of Acoustic Scenes and Events (DCASE) Workshop*, 2023, pp. 51–55.
- [38] K. Shimada, K. Uchida, Y. Koyama, T. Shibuya, S. Takahashi, Y. Mitsuji, and T. Kawahara, "Zero- and few-shot sound event localization and detection," *arXiv preprint arXiv:2309.09223*, 2023.
- [39] Q. Kong, Y. Cao, T. Iqbal, Y. Wang, W. Wang, and M. D. Plumbley, "PANNs: Large-scale pretrained audio neural networks for audio pattern recognition," *IEEE/ACM Transactions on Audio, Speech, and Language Processing*, vol. 28, pp. 2880–2894, 2020.
- [40] A. Politis, "Microphone array processing for parametric spatial audio techniques," Ph.D. dissertation, Aalto University, 2016.
- [41] B. Rafaely, *Fundamentals of Spherical Array Processing*. Springer, 2015.
- [42] A. Politis and H. Gamper, "Comparing modeled and measurement-based spherical harmonic encoding filters for spherical microphone arrays," in *Proceedings of IEEE Workshop on Applications of Signal Processing to Audio and Acoustics (WASPAA)*, 2017, pp. 224–228.
- [43] L. Van der Maaten and G. Hinton, "Visualizing data using t-SNE," *Journal of Machine Learning Research*, vol. 9, no. 86, pp. 2579–2605, 2008.
- [44] A. Politis, "[DCASE2022 Task 3] Synthetic SELD mixtures for baseline training," Apr. 2022. [Online]. Available: <https://doi.org/10.5281/zenodo.6406873>
- [45] A. Mesaros, S. Adavanne, A. Politis, T. Heittola, and T. Virtanen, "Joint measurement of localization and detection of sound events," in *Proceedings of IEEE Workshop on Applications of Signal Processing to Audio and Acoustics (WASPAA)*, 2019, pp. 333–337.
- [46] A. Politis, A. Mesaros, S. Adavanne, T. Heittola, and T. Virtanen, "Overview and evaluation of sound event localization and detection in DCASE 2019," *IEEE/ACM Transactions on Audio, Speech, and Language Processing*, vol. 29, pp. 684–698, 2021.
- [47] I. Loshchilov and F. Hutter, "Decoupled weight decay regularization," in *Proceedings of International Conference on Learning Representations (ICLR)*, 2018.
- [48] S. Ioffe and C. Szegedy, "Batch normalization: Accelerating deep network training by reducing internal covariate shift," in *Proceedings of International Conference on Learning Representations (ICLR)*, 2015.
- [49] A. Varga and H. J. Steeneken, "Assessment for automatic speech recognition: II. NOISEX-92: A database and an experiment to study the effect of additive noise on speech recognition systems," *Speech Communication*, vol. 12, no. 3, pp. 247–251, 1993.
- [50] H. Fu, B. Cai, L. Gao, L.-X. Zhang, J. Wang, C. Li, Q. Zeng, C. Sun, R. Jia, B. Zhao *et al.*, "3D-FRONT: 3D furnished rooms with layouts and semantics," in *Proceedings of IEEE/CVF International Conference on Computer Vision (ICCV)*, 2021, pp. 10 933–10 942.
- [51] Z. Tang, R. Aralikatti, A. Ratnarajah, , and D. Manocha, "GWA: A large geometric-wave acoustic dataset for audio processing," in *Proceedings of Special Interest Group on Computer Graphics and Interactive Techniques Conference (SIGGRAPH)*, no. 36, 2022, pp. 1–9.
- [52] A. Setlur, O. Li, and V. Smith, "Two sides of meta-learning evaluation: In vs. out of distribution," in *Proceedings of Advances in Neural Information Processing Systems (NeurIPS)*, vol. 34, 2021, pp. 3770–3783.
- [53] S. Chen, L.-K. Huang, J. R. Schwarz, Y. Du, and Y. Wei, "Secure out-of-distribution task generalization with energy-based models," in *Proceedings of Advances in Neural Information Processing Systems (NeurIPS)*, 2023.